Electronic Supplement 1. Velocity and porosity derived from seismic data: a sensitivity analysis

To illustrate the spread in determined velocities along line 05CM-04 and the dependence of porosity on the assumed velocity-porosity function, Figure ES1 compares depth profiles of velocity and porosity at shotpoint 2037 (x=-35 km), on the western flank of the seamount and just west of the location of the proposed IODP riser drilling hole (Wallace et al., 2013). High Density Velocity Analysis (HDVA) shown in Figure ES1a is a semi-automated procedure conducting normal moveout velocity analysis on each CDP gather of the profile. Gathers were pre-processed to optimise automated semblance picking, with velocity picks constrained by permitted deviation from a starting Vrms velocity model and by acceptable bounds for resultant interval velocities. The Vrms model was smoothed laterally prior to Dix conversion to interval velocity. The HDVA method allows for, and preserves, high spatial variation in velocity.

Two supporting velocity models are derived from separate pre-stack depth migration (PSDM) velocity analyses using Paradigm Geophysical's GeoDepth software suite. Different layer-based structural models were defined on the time section for each, and horizon-based velocity analysis performed on those structural models; the velocity models are iteratively refined through pre-stack depth migration of the seismic data. Resultant interval velocities at a particular location are an average for a given layer but laterally may vary smoothly within a layer. Velocity variation with depth at length scales shorter than the interval thickness (typically hundreds to thousands of meters) is not preserved.

The long wavelength component of the HDVA-derived velocity is broadly compatible with the coarser interval velocities derived from PSDM (defining the shaded envelope in Figure ES1a).

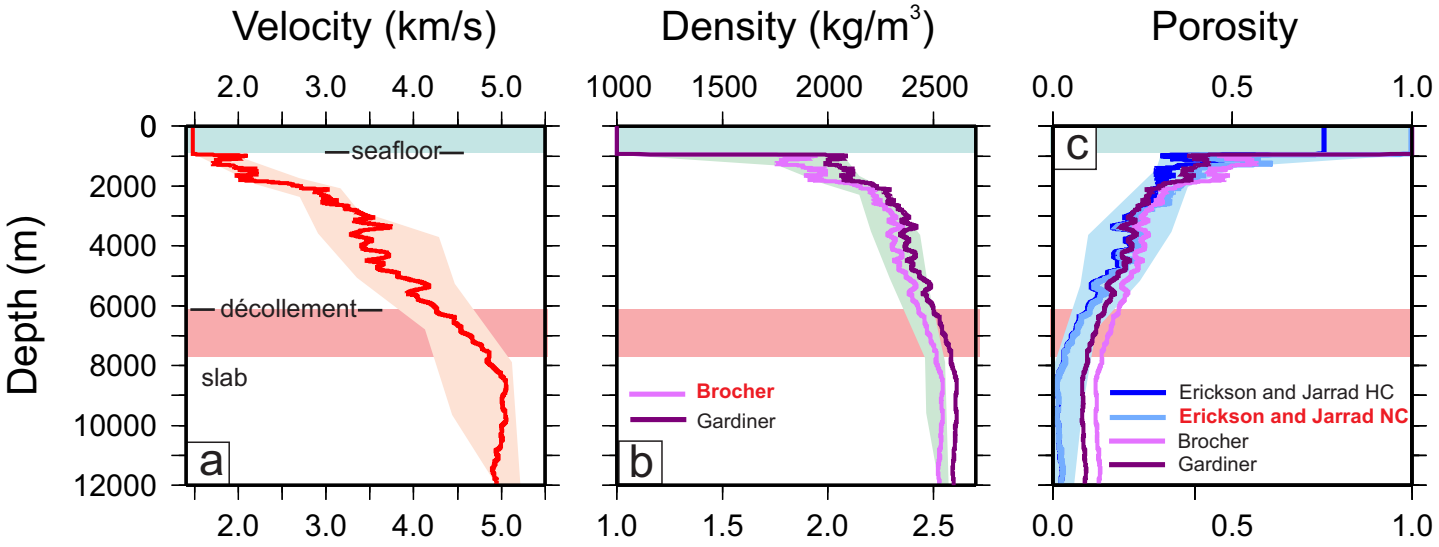

Figure ES1. (a) Velocity determined by High Density Velocity Analysis derived from the multi-channel seismic data along line 05CM-04 at x=-35 km (see Figure 2 for location of this profile). The shaded regions represent the range of velocity functions and transformations derived for this site using two separate pre-stack depth migration velocity analyses. (b) calculated density derived using the relationships of Brocher (2005) and Gardner et al. (1974). Red highlight of reference indicates method used in the main paper for fluid budget analysis. (c) Porosity calculations. The four porosity curves were derived using: Erickson & Jarrard (1998) using normal (NC) and high compaction (HC); Gardner et al. (1974); and Brocher (2005) (assuming a particle density of 2750 kgm^{-3}). Red highlight of reference indicates method used in the main paper. Note that the porosity varies more between transformation methods than from velocity variations alone, i.e. the blue shaded area (c), derived from the range of velocity values (a) using Erickson & Jarrard (1998) normal compaction gives less spread than the porosity values derived from the four different velocity-porosity relationships at depths greater than 4 km.

Electronic Supplement 2. Modelled material deformation: sensitivity to fault friction along décollement

In the main paper we assume a low effective friction angle of 5° along the décollement when computing flow of rock through and beneath the wedge. This is lower than other modelling studies of subduction detachments. For example, Rowe et al. (2012) discuss laboratory experiments and conduct a sensitivity study using fault friction coefficients of =0.25 (base model), 0.15, and 0.35, corresponding to angles of friction (respectively) of 14, 8.5, and 19°. They found that the high-friction case (ϕ = 19°) was not consistent with observed deformation for the Kumano Basin transect of the Nankai subduction zone.

In Figure ES2, we compare our base model results (in terms of velocity fall-off across the trench) to those using a higher friction angle.

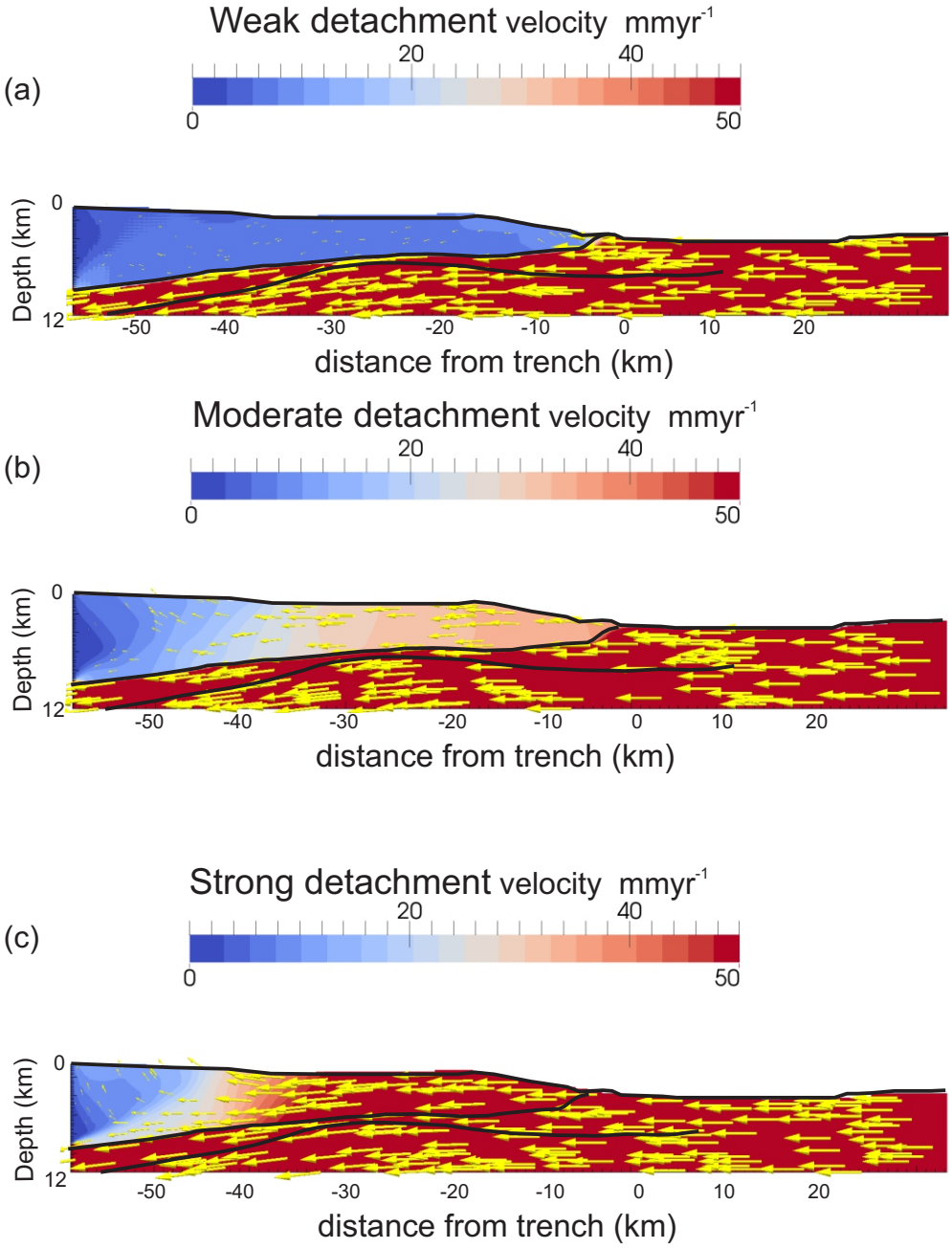

Figure ES2. Comparison between weak, moderate and strong fault friction (angles of friction 1, 5 and 15° respectively. Colour contours are velocity magnitude (0-50 mm/yr) and with velocity vectors at selected points superimposed. The strong detachment case predicts deformation all the way to the backstop, which is not consistent with preliminary structural reconstructions that suggest that most recent deformation has occurred in the frontal part of the wedge (between x = -20 and 0 km).

Electronic Supplement 3. Spatial gradient in porosity

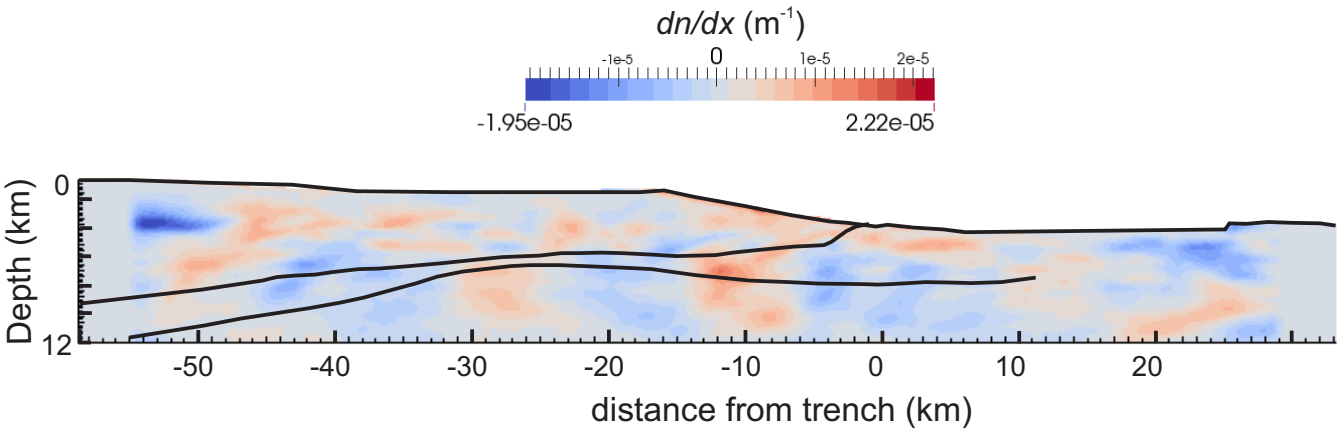

Figure ES3. The horizontal gradient in the porosity field of Fig. 2b (dn/dx).

Electronic Supplement 4. Non-equilibrium wedge mechanics: models of seamount subduction as an explanation for changing taper along profile 05CM-04

As discussed in the main text, assuming steady-state material flow of sediment through the present-day wedge along profile 05CM-04 is not strictly valid since subduction of a seamount is expected to perturb the wedge shape in time. In fact, it is not possible to compute a range of material strengths for the sediment and décollement at a stable or critical stress state that reproduces the change in taper along the profile from a steep frontal wedge to almost flat bathymetry further landward (Bassett et al., 2014). Instead, the seamount perturbs wedge dynamics so that some parts are below critical taper, some parts are stable, and other parts are over-steepened.

Fig. ES4 illustrates how wedge mechanics can change on timescales of 100 ky as a seamount approaches and is subducted beneath the toe of the wedge. Although the dimensions and shape of the seamount are not specifically matched to profile 05CM-04, the model shown here reproduces the main features that we see in that profile. 650 ky after the seamount enters the trench, it is in approximately the location inferred from the present-day profile along 05CM-04. At this time, the model predicts that the wedge will be over-steepened seaward of the seamount and that deformation (high strain-rates) will be focused there, while landward of the seamount the seafloor slope is almost flat. Despite the oversteepened wedge toe, it is not in active extension (although some surface slumping is predicted). The material flow vectors (Fig. ES4(b)) are similar in magnitude to those shown in the paper (Fig. 3) for a moderately weak detachment starting from the present-day bathymetry. This gives us some confidence that our assumed material flow-field in the paper is roughly correct for timescales of thousands of years over which fluid release from compaction is expected to occur, even though it has been derived assuming steady-state flow.

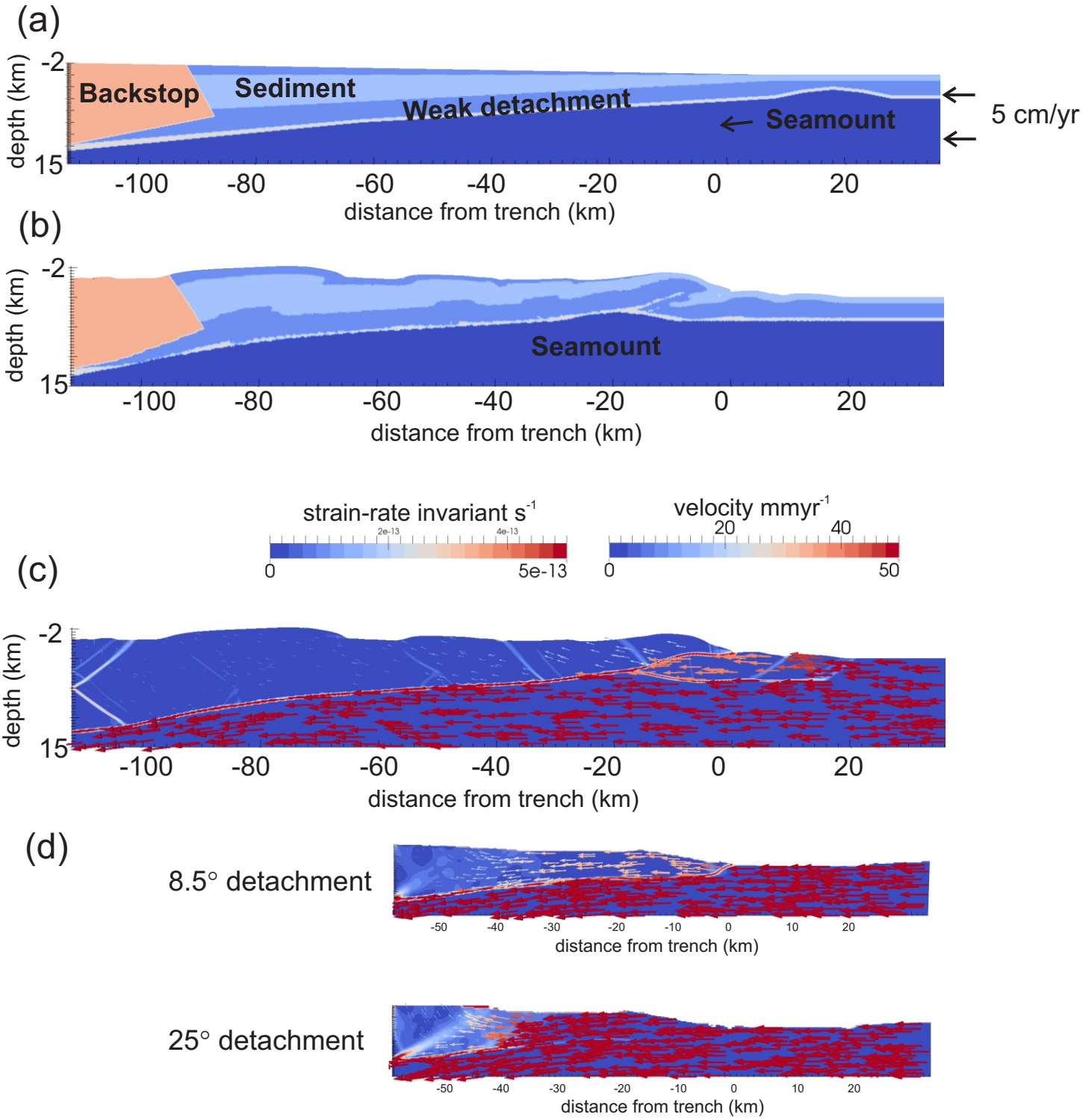

Figure ES4. (a) initial setup of numerical experiment with subducting seamount. Backstop (red), sediment (blue, yellow layers) and slab (white) have dry friction angles of 35°, 30°, and 30° respectively, while weak detachment has a dry friction angle of 8°. Hydrostatic fluid pressure is assumed, so that these correspond to effective friction coefficients of 20°, 17.5° and 4.8°, respectively. Cohesion is 1 MPa for all material except detachment where it is negligible. A boundary velocity of 5 cm/yr is applied along the right-hand edge of the model and at the base and below of the backstop parallel to the detachment layer. An initial taper of 1° is applied at the top of the model (which is a free surface). (b) Geometry after 1 My of deformation. The seamount has created, and then passed landward of, a steep frontal wedge. (c) Strain-rate invariant (colour contours) and velocity vectors after 1 My. (d) Nominal model from the main paper (Fig. 3), and equivalent for a higher detachment strength, using present-day geometry and inferred materials at depth for comparison. Dry friction angles along detachment labelled to left of panels are for a fluid pressure ratio λ=0.65.